RESEARCH PAPER

Evolution of Ordovician YJ1X ultra-deep oil reservoir in the Yuecan oilfield, Tarim Basin, NW China

YANG Peng[1], LIU Keyu[1, 2, *], LI Zhen[3], MCINNES Brent Ian Alexander[3], LIU Jianliang[1]

1. Key Laboratory of Deep Oil and Gas, China University of Petroleum, Qingdao 266580, China;
2. Qingdao National Laboratory for Marine Science and Technology, Qingdao 266071, China;
3. John de Laeter Centre, Faculty of Science and Engineering, Curtin University, Perth, WA 6485, Australia

Abstract: Based on a combined *in-situ* calcite U-Pb dating, molecular geochemical correlations of reservoir oil and extract from reservoir rocks, and fluid inclusion analysis, the charge and evolution history of the YJ1X ultra-deep oil reservoir of the Ordovician Yijianfang Formation in the southwestern part of the Tabei Uplift has been determined systematically. (1) The reservoir oil, free oil and inclusion oil have similar geochemical characteristics and are presumably derived from marine source rock deposited in similar sedimentary environment. (2) The reservoir oil, free oil and inclusion oil have similar maturities with calculated equivalent vitrinite reflectance values in the range of 0.80%–0.96%. (3) Two types (Group I and II) of oil inclusion assemblages (OIAs) have been identified in the reservoir, of which Group I represents the original gas-saturated oil entering the trap during the initial oil charge, whereas Group II represents undersaturated residual oil retained in the reservoir after minor leakage of light hydrocarbon. (4) The reservoir experienced oil charge only once during the Early Devonian around 425 Ma and has been well preserved after the minor light hydrocarbon leakage in the Middle Devonian. The study shows that there may be old oil and gas accumulations in ultra-deep strata of petroliferous basins with well-developed caprock and stable tectonic background.

Key words: oil accumulation and preservation; *in-situ* calcite U-Pb dating; fluid inclusion; Ordovician; ultra-deep reservoir; carbonate reservoir; Tarim Basin

Introduction

Petroleum systems capable of forming oil accumulations range from Archean to Neogene [1], including oil preserved in fluid inclusions in sandstones of *ca.* 2.9 Ga old [2], "live" oil shows reported in sedimentary rocks of *ca.* 1.4 Ga old [3]. However, almost all reported reservoir oils that have been produced commercially are younger than 400 Ma [4–6]. According to Miller [5], the median age for oil accumulations is only approximately 29 Ma, and over 75% of oil accumulations globally were charged within the last 75 Ma. Indeed, oil accumulations in geological history have been subject to various types of destruction and alteration, such as biodegradation and water washing, evaporative fractionation, thermal sulfate reduction (TSR), thermal cracking, tectonic activity, and fault leakage [7]. Tectonic reactivation and sealing capability are

two fundamental factors impacting oil preservation after entrapment [8–9]. Thermal cracking exerts a significant effect on oil accumulation in the deep and ultra-deep reservoirs, often promoting the conversion of oil to condensate or gas [4, 8]. The temperature at which oil cracking begins is generally believed to be greater than 160 °C [10–12].

The carbonate platform area of the Tarim Basin shows huge resource potential and is an important exploration frontier for deep and ultra-deep oil and gas exploration in China [13–15]. The marine carbonate strata in the carbonate platform area are commonly situated in the lower stratigraphic interval of the Tarim Basin with old ages and large burial depths. After multiple cycles of tectonic activity, marine carbonate reservoirs have undergone complex destruction and alteration [15–16]. The discovery of the

Shunbei–Yuecan oilfield marks a major breakthrough in the oil and gas exploration of ultra-deep marine carbonate rocks in the Tarim Basin in recent years [17–19]. The target reservoir layers are the middle–lower Ordovician Yijianfang and Yingshan formations with burial depths of over 7000 m. Different from the weathering crust reservoirs in the Tahe area, the Ordovician reservoirs in the Shunbei–Yuecan area are characterized by the faulting-karsting type, characterized by pervasive occurrence of oil but isolated distribution of commercial oil accumulations along the fault zone [17]. Yang et al. [20] indicated that the Shunbei area mainly experienced two significant oil charge events, of which the first occurred during the late Caledonian Orogeny and the second during the mid-Hercynian Orogeny, respectively, and the oil reservoirs have been well preserved since then. In comparison, the understanding of the charge and evolution history of the Ordovician reservoirs in the Yuecan area is relatively limited.

Oil-bearing fluid inclusions are small aliquots of geofluids entrapped in rock-forming minerals [21], such as quartz, feldspar and calcite, which record the geological information related to oil reservoir formation, alteration and destruction (biodegradation and water washing, evaporative fractionation, thermal cracking, TSR, and fault leakage, etc.) [22–23], and are generally not affected by subsequent geological processes after trapping. Detailed fluid inclusion analysis can help deciphering geochemical fingerprints of oil charged at different times, and reveal the charge history and secondary alteration process of oil reservoirs. At the same time, *in-situ* laser-ablation U-Pb dating of carbonates is a high-precision dating method developed for minerals with low U contents, which can achieve accurate dating of multi-generation calcite cements. It has been widely used in delineating faulting events and reconstructing fluid evolution history [24–27]. In particular, when oil charge event coincides with the formation of calcite cement, a small amount of oil droplets can be entrapped in the lattice defects of calcite as primary fluid (oil) inclusions [28]. In this case, the timing of oil charge event can be obtained indirectly by determining the formation timing of calcite cement containing primary fluid (oil) inclusions. In addition, the Ordovician Yijianfang Formation reservoir in Well YJ1X has a continuous coring interval of nearly 90 m, which provides abundant materials for studying the charge and evolution history of the reservoir in this area. Hence, by integrating *in-situ* calcite U–Pb dating, molecular composition characteristics of hydrocarbons, and fluid inclusion analysis, the charge and evolution history of the Ordovician ultra-deep reservoir in Well YJ1X in the Yuecan area can be elucidated. The work can also offer an in-depth understanding of the evolution process of the Ordovician ultra-deep reservoir in the Tarim Basin and provide a reference for future ultra-deep oil and gas exploration in the area.

1. Geological background

The Yuecan area is located in the southwestern part of the Tabei Uplift in the northern Tarim Basin, adjacent to the Shuntuoguole Low Uplift, and between the Awati Depression and the Manjiaer Depression along the east-west direction (Fig. 1a). The strata encountered in the study area sequentially from top to bottom include Quaternary, Neogene, Paleogene, Lower Cretaceous, Lower Jurassic, Triassic, Lower Permian, Lower Carboniferous, and Upper Devonian, Lower Silurian and Ordovician strata. Similar to the Shunbei area, the Lower Paleozoic marine carbonate strata in the Yuecan area constitute a complete source-reservoir-cap rock assemblage (Fig. 1b). The reservoirs rocks are composed mainly of the
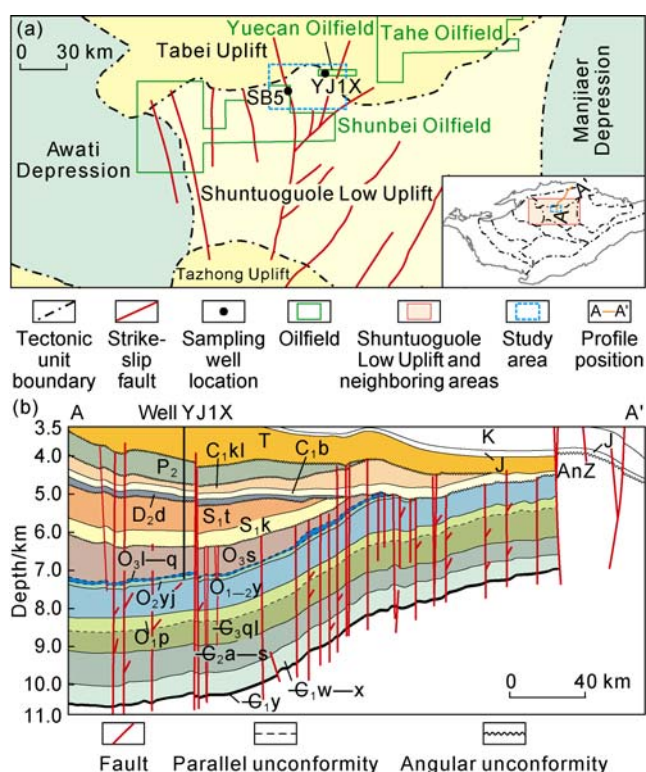

Fig. 1. Maps showing major tectonic units in the Tarim Basin and location of the study area (a), and a near NE trending structural-stratigraphic section through AA' (b) (modified from Reference [18]). K—Cretaceous; J—Jurassic; T—Triassic; P_2—Middle Permian; C_1kl—Lower Carboniferous Kalashayi Formation; C_1b—Lower Carboniferous Bachu Formation; D_3d—Upper Devonian Donghetang Formation; S_1t—Lower Silurian Tataerertage Formation; S_1k—Lower Silurian Kepingtage Formation; O_3s—Upper Ordovician Sangtamu Formation; O_3l—q—Upper Ordovician Lianglitage and Qiaerbake formations; O_2yj—Middle Ordovician Yijianfang Formation; $O_{1-2}y$—Middle–Lower Ordovician Yingshan Formation; O_1p—Lower Ordovician Penglaiba Formation; Є_3ql—Upper Cambrian Xiaqiulitage Group; Є_2a—s—Middle Cambrian Awatage and Shayilike formations; Є_1w—x—Lower Cambrian Wusonggeer and Xiaoerbulake formations; Є_1y—Lower Cambrian Yuertusi Formation; AnZ—Pre-Sinian.
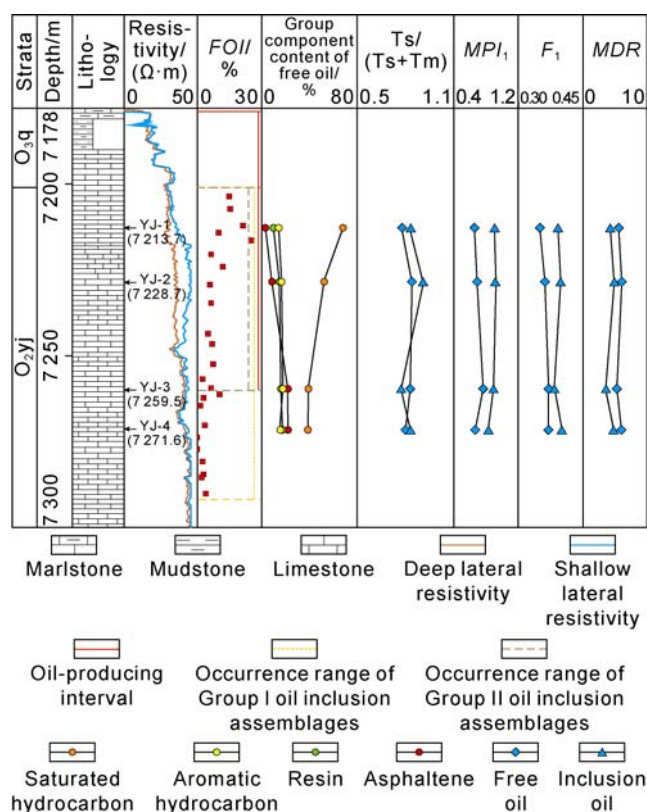
Fig. 2. Generalized stratigraphic column of the Ordovician Yijianfang Formation for Well YJ1X.

Ordovician Yijianfang Formation (O_2yj) and the upper part of the Yingshan Formation ($O_{1-2}y$), and the reservoir space types are dominated by fault-related dissolution caves, vugs, dissolution pores and fractures [17, 19]. The overlying Upper Ordovician Sangtamu Formation (O_3s) mudstone and limestone serve as regional cap rocks, and the Lower Cambrian Yuertusi Formation ($\in_1y$) shale is considered as the main source rock in the study area [17–19, 29–31]. The main oil-bearing layer of Well YJ1X (Fig. 1a) is within the Ordovician Yijianfang Formation at the depth interval between 7178.54 m and 7260.00 m (Fig. 2). The current reservoir formation temperature is 155.27 °C with a calculated geothermal gradient of 21.5 °C/km. The corresponding formation pressure of the reservoir is 81.83 MPa with an estimated pressure coefficient of 1.13. The reservoir formation water is typical of a $CaCl_2$ type, and has salinity values of 152 358–173 493 mg/L.

2. Samples and methods

Thirty core samples in the Yijianfang Formation (O_2yj) were collected from the oil-bearing carbonate rocks of Well YJ1X over the depth interval of 7203.60 m to 7290.18 m (Fig. 1a). Analyses performed on these reservoir rocks include sequential Soxhlet extraction, calcite vein petrography, in-situ calcite U-Pb dating and fluid inclusion analysis. Because the calcite veins in the carbonate reservoirs in Well YJ1X are too fine to be dated using the in-situ calcite U-Pb dating technique, and considering

that the Shunbei area and the Yuecan area share similar sedimentary environment and fluid evolution history, five core samples of the Ordovician Yijianfang Formation in Well SB5 (Fig. 1a) in the Shunbei area were selected (sampling depth: 7331.27 m to 7427.30 m) to assist in calcite vein characterization and in-situ calcite U-Pb dating. The oil sample used in this study was collected from the Ordovician oil layer in Well YJ1X (Fig. 2). The geochemical characteristics of the Ordovician reservoir oils in the Shunbei area are based on Yang et al. [20].

Sequential Soxhlet extraction experiments of crushed carbonate core samples were carried out at the State Key Laboratory of Organic Geochemistry, Guangzhou Institute of Geochemistry, Chinese Academy of Sciences. Following the procedure of Yu et al. [32], four carbonate core samples from Well YJ1X (Fig. 2) were sequentially extracted to obtain the free (extractable adsorbed) oils and inclusion oil extracts. The free oil and inclusion oil extracts from top to bottom in the present study are named as YJ-1A, YJ-2A, YJ-3A, YJ-4A and YJ-1B, YJ-2B, YJ-3B, YJ-4B, respectively. The free oils, inclusion oils and reservoir oil from Well YJ1X were then used for gas chromatography (GC) and gas chromatography-mass spectrometry (GC-MS) analyses. Detailed experimental procedure follows that of Yang et al. [20].

In-situ calcite U-Pb dating was performed at the John de Laeter Centre, Curtin University, Perth, Australia, after an initial screening and identification of high-purity calcite grains via Tescan Integrated Mineral Analyzer (TIMA). Ablations utilized an ASI RESOlution-SE 193 nm excimer laser, and elemental abundances were determined using an Agilent 8900 QQQ quadrupole ICP-MS operated in single quad mode. Parameters include 10 Hz repetition rate, 4 J·cm⁻² laser energy, 87 μm spot diameter and 60 s ablation time at each data point. Raw data were processed using the Iolite 3.7 software. A natural calcite sample, WC-1 ((254.4±6.4) Ma), was used as the main reference standard [33]. U-Pb Tera-Wasserburg concordia plots were obtained using the IsoplotR program [34].

Ten core samples were characterized petrographically using a Zeiss Axio Imager A2m optical microscope and imaged by a Relion III cold-cathode device with beam voltages of up to 15 keV and an electric current of 500 μA. Twenty-five core samples were prepared as doubly polished wafers with approximately 80 μm in thickness for fluid inclusion petrography, fluorescence spectroscopy and microthermometry. Fluid inclusion petrography was carried out according to the FIA (Fluid Inclusion Assemblage) method proposed by Goldstein and Reynolds [21]. The abundance of oil inclusions in carbonate samples at different depths was characterized by the FOI (Frequency of Oil Inclusion) technique proposed by Eadington et al. [35]. Fluorescence spectra of both oil inclusions and reservoir oil were obtained using a Horiba iHR320 im-

aging spectrometer. Microthermometry measurements of fluid inclusions were conducted on a Linkam THMSG600 heating-freezing stage using the cycling technique proposed by Goldstein and Reynolds [21]. The measurement precision is ±1 °C for the homogenization temperature (Th) and ±0.1 °C for the final ice melting temperature (Tm), respectively. The NaCl- equivalent salinity of aqueous inclusions was calculated based on an equation proposed by Bodnar [36].

3. Petroleum geochemical characteristics

The Ordovician ultra-deep oil reservoir in Well YJ1X of the Yuecan area is presently an undersaturated volatile oil reservoir overall. The reservoir oil has a density of 0.813 g/cm³, a viscosity of 3.25 mPa·s, a sulfur content of 0.20%, a wax content of 4.70%, and a production gas-oil ratio (GOR) of 141 m³/m³. It is classified as a light oil with low viscosity and low sulfur content. The abundances of saturated hydrocarbons, aromatic hydrocarbons, resin and asphaltene in the reservoir oil are 77.8%, 11.6%, 7.6% and 3.0%, respectively. In comparison, the abundances of saturated hydrocarbon, aromatic hydrocarbon, resin and asphaltene in the free oil obtained by core extraction are in the range of 41.0%–70.5%, 15.1%–18.9%, 10.5%–18.8% and 3.9%–23.6%, respectively. The abundances of the saturated hydrocarbons in the free oils gradually decrease with depth from 70.5% to 41.0%, while the abundances of resin and asphaltene show an opposite trend (Fig. 2).

The ratios of pristane/phytane for the oil, free oils and inclusion oils are all falling in the range of 0.30–0.92, indicating that the source rocks were deposited predominantly under anoxic conditions [1, 37]. The ratios of pristane/nC$_{17}$ and phytane/nC$_{18}$ for the reservoir oil, free oils and inclusion oils range from 0.14 to 0.44, and 0.21 to 0.50, respectively, showing that the corresponding organic materials are dominated by marine organic matter (Type II) [38], which is similar to the geochemical characteristics of the Ordovician reservoir oils in the Shunbei area (Fig. 3). Abundant sterane compounds, including C$_{21}$ pregnane, C$_{22}$ homopregnane, diasterane, and C$_{27}$–C$_{29}$ regular steranes are detected in the reservoir oil, free oils and inclusion oils, and the relative abundances of C$_{27}$, C$_{28}$ and C$_{29}$ regular steranes show a typical V-shape distribution pattern. It can be seen from Fig. 4 that the relative content of C$_{29}$ regular sterane is the highest among the C$_{27}$–C$_{29}$ regular steranes, similar to the geochemical characteristics of Ordovician reservoir oils in the Shunbei area, indicating that green algae would be an important source for the organic matter [39]. The relative abundance of C$_{23}$TT (C$_{23}$ tricyclic terpene) in the reservoir oil of the Yijianfang Formation is the highest among all the terpenoids, and the values of C$_{20}$/C$_{23}$TT (ratio of C$_{20}$TT to C$_{23}$TT) and C$_{23}$TT/(C$_{23}$TT+C$_{30}$H) are 0.57 and 0.81, respectively. The values of C$_{20}$/C$_{23}$TT and C$_{23}$TT/(C$_{23}$TT+C$_{30}$H) for the

free oils are in the range of 0.24–0.51 and 0.33–0.65, respectively. The terpene distribution of the inclusion oils is similar to that of the free oils, with corresponding values in the range of 0.26–0.99 and 0.21–0.65, respectively. It is worth noting that the relative content of tricyclic terpenes in the free oils and inclusion oils gradually decreases with depth, while the relative content of pentacyclic triterpenes shows an opposite trend. The values of C$_{23}$TT/(C$_{23}$TT+C$_{30}$H) in the free oils and inclusion oils decrease from 0.65 to 0.33 and 0.21, respectively, comparable to the trend of the relative content of saturated hydrocarbons in free oils decreasing with depth, while the relative content of resin and asphaltene increasing with depth (Fig. 2). The cross plot of DBT/P (dibenzothiophene/phenanthrene) and Pr/Ph indicates that the reservoir oil, free oils and inclusion oils are mainly located close to Zone 2 and Zone 3, similar to that of the reservoir oils in the Shunbei area (Fig. 5), manifesting that the corresponding source rocks may be shales deposited in a marine environment [40]. In summary, the geochemical characteristics of the oil, free oils and
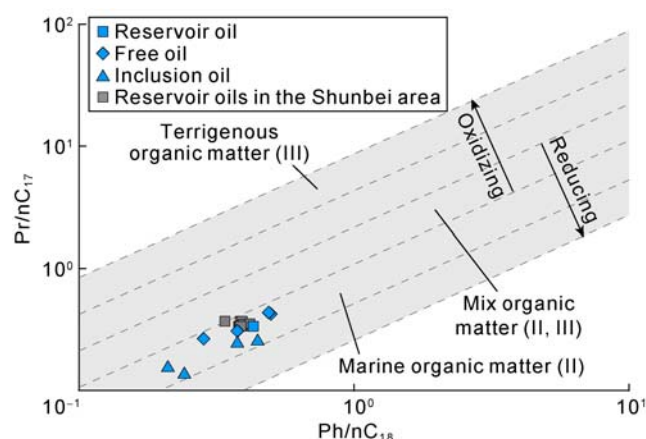
Fig. 3. Cross plot of Ph/nC$_{18}$ and Pr/nC$_{17}$ for the reservoir oil, free oils and inclusion oils (modified from Reference [38]).
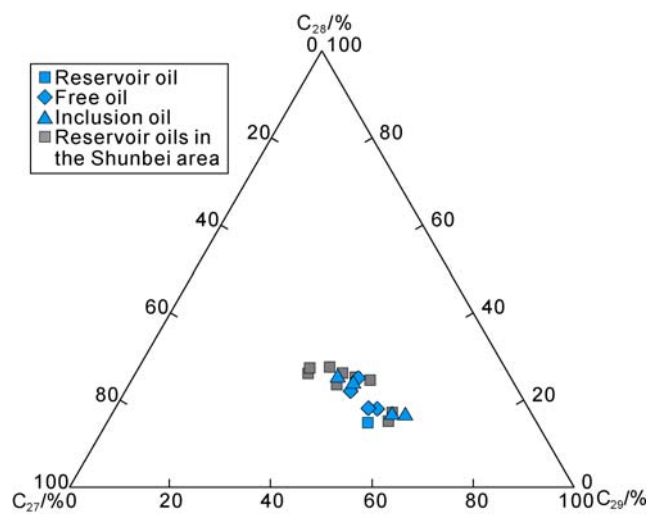
Fig. 4. Triangular plot of the relative proportions of C$_{27}$–C$_{29}$ regular steranes for the reservoir oil, free oils and inclusion oils.
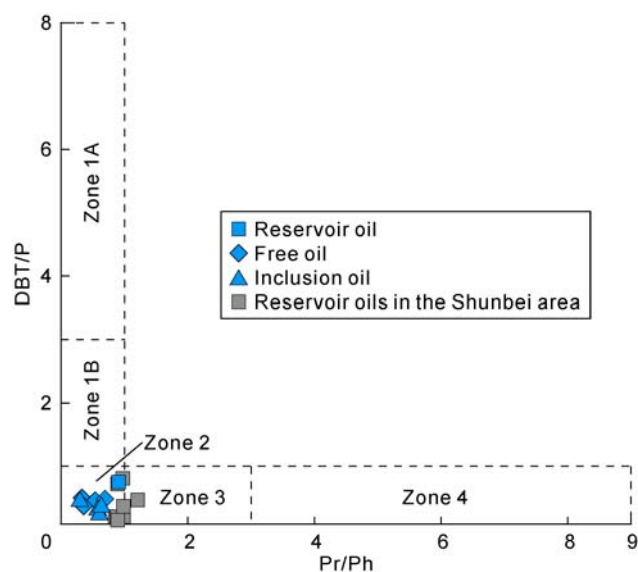
Fig. 5. Cross plot of Pr/Ph and DBT/P for the reservoir oil, free oils and inclusion oils (modified from reference [40]).

inclusion oils are similar to those of the reservoir oils in the Shunbei area, and they can be classified as one oil family. It is speculated that they were derived from marine source rocks deposited under similar depositional environments. The isomerization ratios of $C_{29}\beta\beta/(\beta\beta+\alpha\alpha)$ and $C_{29}20S/(20S+20R)$ for the oil, free oils and inclusion oils are in the range of 0.47–0.57 and 0.45–0.55, respectively, indicating that the maturity of the source rock generating these oils would be close to or even greater than that of the peak stage of oil generation. Therefore, these parameters cannot be used as effective maturity indicators[1]. MPI_1 and F_1 are common thermal maturity indicators used for characterizing high-mature hydrocarbons [41-42]. The cross plot of MPI_1 and F_1 shows that the oil, free oils and inclusion oils are all located in the lower left region, close to that of the early charged oil in the Shunbei area (Fig. 6). Based on the correlation of methylphenanthrene index MPI-1 and vitrinite reflectance [43-44], the calculated equivalent vitrinite reflectance values of the oil, free oil and inclusion oil range from 0.80% to 0.96%, comparable to that of the corresponding source
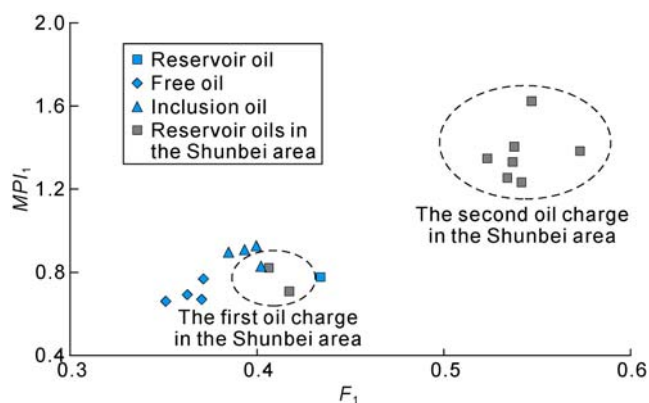
rocks for the early charged oil in the Shunbei Ordovician oil reservoir [20]. In addition, the values of Ts/(Ts+Tm), MPI_1, F_1, and MDR for the free oils are quite close to that for the inclusion oils. These values vary less apparently in the vertical profile (Fig. 2), indicating that the hydrocarbons in the Ordovician reservoir in Well YJ1X have relatively consistent maturity.

4. Calcite cement U-Pb dating

Two generations of calcite cement (sequentially named as C1 and C2) based on paragenetic relationships were identified in the carbonate samples (Fig. 7a). The C1 calcite cement occurs as fracture fillings, mostly medium-coarse crystalline, and is characterized by blocky or mosaic aggregates with dark red cathodeluminescence or nonluminescence. The C2 calcite cement also occurs as fracture fillings and intersects the C1 calcite cement (Fig. 7b). It is composed mainly of blocky or mosaic calcite aggregates with orange cathodeluminescence. *In-situ* calcite U-Pb dating results show that the formation ages of C1 and C2 calcite cements are (446.1±4.4) Ma (Fig. 8a) and (425.7±14.0) Ma (Fig. 8b), respectively. These age results have verified the paragenetic relationships observed of calcite cements and provided constraints on the oil charge timing.

5. Fluid inclusion types and genesis

Fig. 2 shows the variation trend of frequency of oil inclusion (*FOI*) with depth in the reservoir in Well YJ1X. Oil inclusions are composed predominantly of diphasic (L_{oil}-V) and triphasic (S_{bit}-L_{oil}-V or L_{oil}-L_w-V) fluid inclusions, and a small number of multiphasic (S_{bit}-L_{oil}-L_w-V) and monophasic (L_{oil}) oil inclusions are also present (Fig. 9). Oil inclusions are commonly colorless or yellowish under plane-polarized light. Their fluorescence colors are dominated by yellowish white, near white, blue white and bright blue. Bitumen in oil inclusions usually occurs along the walls of oil inclusions or is suspended in the oil inclusions. Oil inclusions are primarily ellipse, elongated, square or irregular in shapes, 5–15 μm in diameters with vapor filling degrees varying from 5% to 20%. Two types of oil inclusion assemblages have been identified on the

Fig. 6. Cross plot of *MPI*-1 and *F*1 for reservoir oil, free oils and inclusion oils (modified from reference [20]).
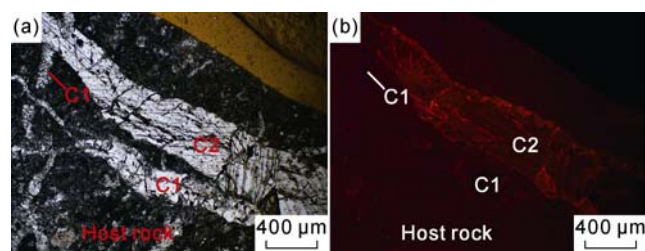

Fig. 7. Petrographic characteristics of calcite cement types in the study area. (a) Well SB5, 7427.30 m, O₂yj, occurrence and paragenesis relationship of C1 and C2 calcite cements, transmitted light; (b) Well SB5, 7427.30 m, O₂yj, occurrence and paragenesis relationship of C1 and C2 calcite cements, cathodoluminescence.
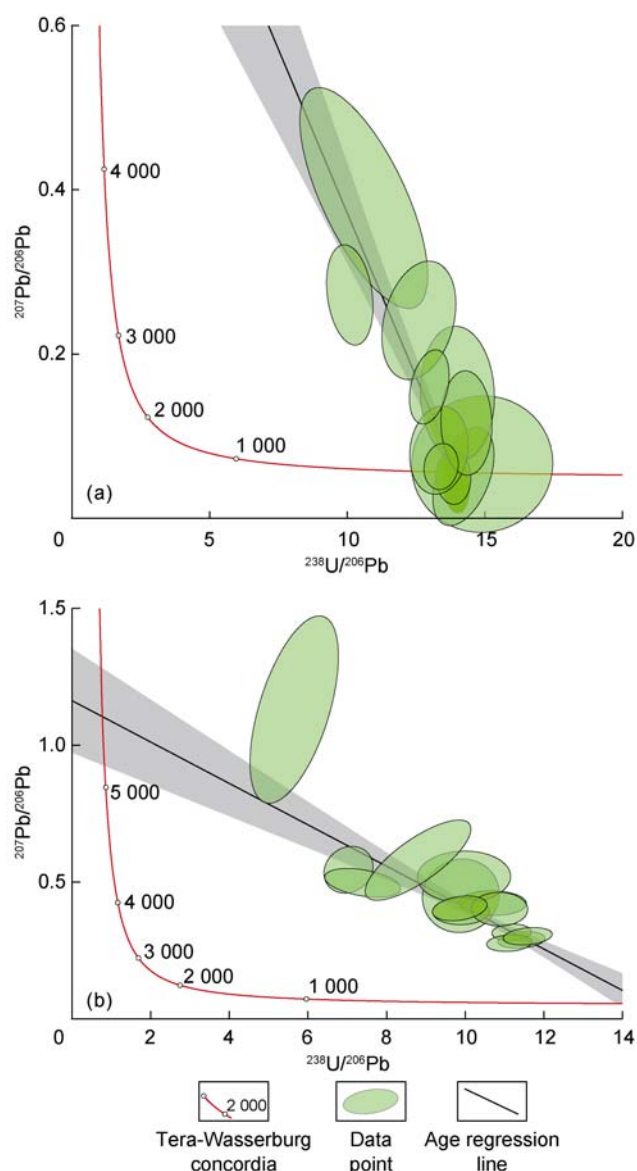
Fig. 8. U-Pb isotopic ages of C1 (a) and C2 (b) calcite cements in the study area. (a) Well YJ1X, 7234.71 m, O_2yj, micritic arenaceous limestone, U-Pb isotopic age is (446.1± 4.4) Ma, MSWD is 2.5, sample number is 12; (b) Well SB5, 7425.00 m, O_2yj, micritic limestone, U-Pb isotopic age is (425.7±14.0) Ma, MSWD is 3.4, sample number is 14.

basis of differences in vapor filling degrees, fluorescence color and bitumen content in oil inclusions: Group I and II oil inclusion assemblages (Figs. 2 and 9). Group I oil inclusion assemblages are widely distributed, and were identified in almost all core samples. The occurrence range of Group II oil inclusion assemblages is relatively limited, which is confined to the current oil-producing interval.

Group I oil inclusion assemblages are characterized by bright blue fluorescing, diphasic (L_{oil}-V) fluid inclusions at room temperature with vapor filling degrees greater than 10% (Fig. 9a–9b). Most of Group I oil inclusion assemblages occur along annealed microfractures within calcite cements, and a small amount is concentrated along the growth zone of the C2 calcite cement or scat-

tered within the calcite crystal (Fig. 9c), typical of primary fluid inclusions [21]. Group II oil inclusion assemblages emit blue-white, near-white and yellow-white fluorescence, have a vapor filling degrees of less than 5%, and are diphasic (S_{bit}-L_{oil}) or triphasic (S_{bit}-L_{oil}-V) at room temperature (Fig. 9d–g). Group II oil inclusion assemblages are mainly present along trails cutting across calcite crystal fabrics. Group II oil inclusion assemblages intersect Group I oil inclusion assemblages (Fig. 9h). The bitumen content in Group II oil inclusions increases with depth, while the vapor filling degrees decrease with depth. In the upper part of the reservoir in Well YJ1X, Group II oil inclusion assemblages are commonly composed of triphasic (S_{bit}-L_{oil}-V) fluid inclusions (Fig. 9d–9e); while in the lower part of the oil reservoir, Group II oil inclusion assemblages mainly consist of diphasic (S_{bit}-L_{oil}) fluid inclusions (Fig. 9f–9g), and often coexist with reddish-brown fluorescing solid bitumen in the pores.

The fluorescence spectral characteristics of the oil inclusions and oil investigated show systematic variations (Fig. 10). The λ_{max} and QF_{535} values of Group I oil inclusions are in the range of 533.33–540.64 nm and 1.46–1.68, respectively. Comparatively, the λ_{max} and QF_{535} values of Group II oil inclusions are 538.03–560.95 nm and 2.30–3.17, respectively. In addition, the λ_{max} and QF_{535} values of the oil are 537.93 nm and 2.00, which are closer to that of Group II oil inclusions (Fig. 10a). Following the correlation between the QF535 parameter and the relative density of oils derived from the Tabei Ordovician oil reservoirs (Fig. 10b), the estimated relative densities of Group I and II inclusion oils are 0.808–0.815 g/cm^3 and 0.825–0.862 g/cm^3, respectively. Microthermometric measurements were carried out on 10 fluid inclusion assemblages, including a total of 133 oil inclusions and 63 aqueous inclusions (Table 1, Figs. 9i–9l and 11). Group I oil inclusions have T_h values ranging from 87.2 °C to 116.9 °C, with a mode of 90–95 °C (Fig. 11a). The coeval aqueous inclusions have T_h values of 90.5–115.6 °C, with T_m values between −7.5 °C and −3.5 °C (Fig. 11b). The obtained equivalent NaCl salinity lies in the range of 5.7%–11.1%, with an average of 8.5%. Group II oil inclusions have a wide range of T_h values, ranging from 28.0 °C to 70.2 °C with a mode of 50–55 °C (Fig. 11a). The T_h and T_m values of coeval aqueous inclusions are 85.2 to 111.5 °C and −14.9 °C to −14.2 °C (Fig. 11b), respectively. The equivalent NaCl salinities range from 18.0% to 18.6%, with an average of 18.3%.

Fluorescence color of inclusion oil has been widely used as a thermal maturity indicator [45], and generally exhibits a change from yellow to blue with increasing thermal maturity, and the corresponding fluorescence spectra exhibiting a "blue shift". It can be seen from Fig. 10a that the fluorescence spectra of Group I inclusion oil show an obvious "blue shift" compared with those of
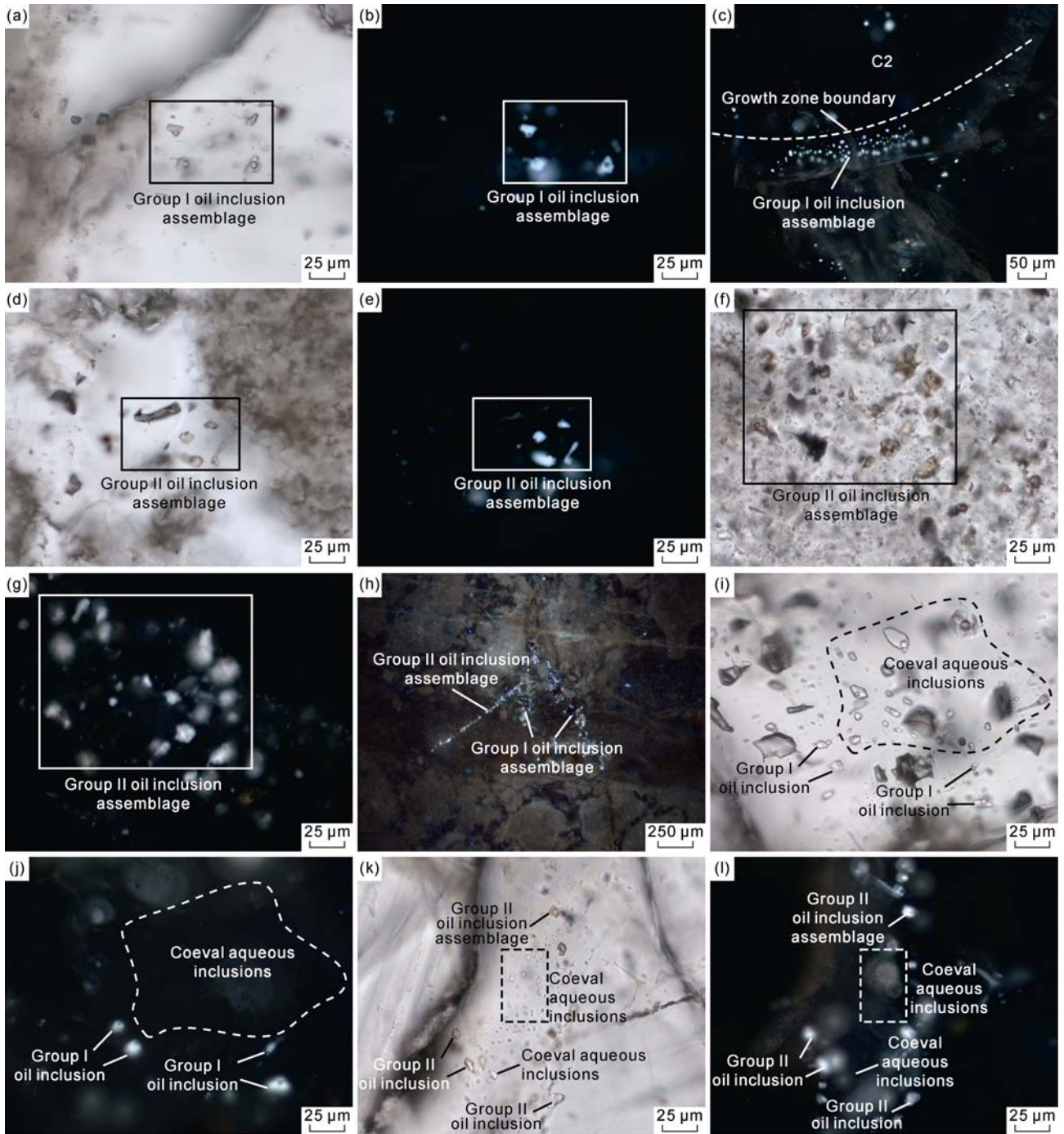
Fig. 9. Petrographic characteristics of oil inclusions from the Ordovician Yijianfang Formation in Well YJ1X. (a) Sample from 7229.30 m, bright blue fluorescing, diphasic (L_{oil}-V) Group I oil inclusions with vapor filling degrees greater than 10%, λ_{max} = 533.59 nm, QF_{535} = 1.46, transmitted light; (b) Sample from 7229.30 m, bright blue fluorescing, diphasic (L_{oil}-V) Group I oil inclusions with vapor filling degrees greater than 10%, λ_{max} = 533.59 nm, QF_{535} = 1.46, UV fluorescence; (c) Sample from 7213.68 m, some bright blue fluorescing Group I oil inclusions occurring along the growth zone of C2 calcite cement, showing typical characteristics of primary fluid inclusions, UV fluorescence; (d) Sample from 7213.68 m, blue-white fluorescing, triphasic (S_{bit}-L_{oil}-V) Group II oil inclusions with vapor filling degrees less than 5% and some bitumen occurring along the walls of oil inclusions, λ_{max} = 538.03 nm, QF_{535} = 2.30, transmitted light; (e) Sample from 7213.68 m, blue-white fluorescing, triphasic (S_{bit}-L_{oil}-V) Group II oil inclusions with vapor filling degrees less than 5% and some bitumen occurring along the walls of oil inclusions, λ_{max} = 538.03 nm, QF_{535} = 2.30, UV fluorescence; (f) Sample from 7259.52 m, near-white fluorescing, diphasic (S_{bit}-L_{oil}) or triphasic (S_{bit}-L_{oil}-V) Group II oil inclusions with high bitumen content and vapor filling degrees less than 5%, λ_{max} = 555.49 nm, QF_{535} = 3.03, transmitted light; (g) Sample from 7259.52 m, near-white fluorescing, diphasic (S_{bit}-L_{oil}) or triphasic (S_{bit}-L_{oil}-V) Group II oil inclusions with high bitumen content and vapor filling degrees less than 5%, λ_{max} = 555.49 nm, QF_{535} = 3.03, UV fluorescence; (h) Sample from 7220.51 m, one blue-white fluorescing Group II oil inclusion assemblage intersecting another bright blue fluorescing Group I oil inclusion assemblage, UV fluorescence; (i) Sample from 7229.30 m, bright blue fluorescing Group I oil inclusions and coeval aqueous inclusions, transmitted light; (j) Sample from 7229.30 m, bright blue fluorescing Group I oil inclusions and coeval aqueous inclusions, UV fluorescence; (k) Sample from 7261.32 m, blue-white fluorescing Group II oil inclusions and coeval aqueous inclusions, transmitted light; (l) Sample from 7261.32 m, blue-white fluorescing Group II oil inclusions and coeval aqueous inclusions, UV fluorescence.
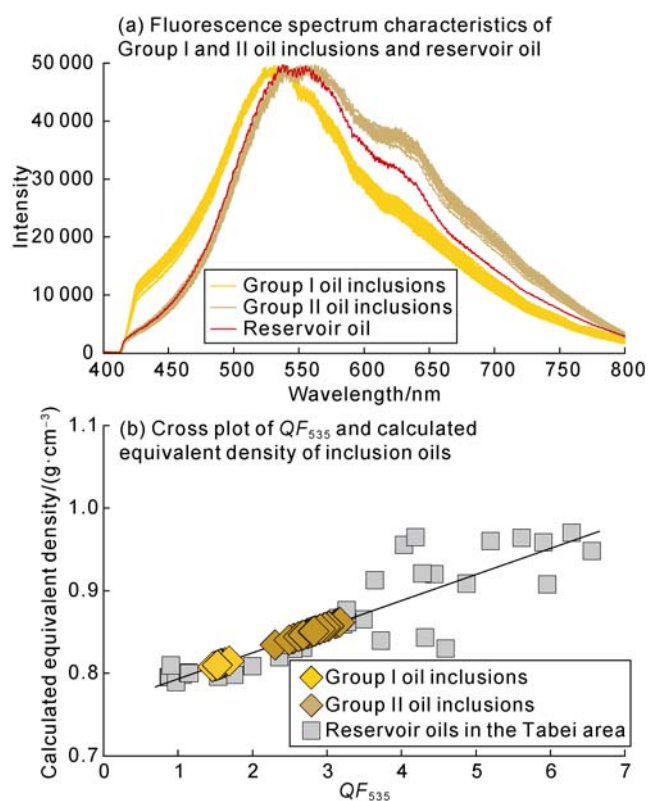
Fig. 10. Fluorescence characteristics and densities of oil inclusions and reservoir oil.

Table 1. Microthermometric data of fluid inclusions from the Ordovician ultra-deep reservoir in Well YJ1X

Type	Oil inclusions	Coeval aqueous inclusions		
	T_h/°C	T_h/°C	T_m/°C	Salinity/%
Group I	87.2–116.9 (79)	90.5–115.6 (26)	−7.5−−3.5 (9)	5.7–11.1 (8.5)
Group II	28.0–70.2 (54)	85.2–111.5 (37)	−14.9−−14.2 (10)	18.0–18.6 (18.3)

Note: The numerator represents the value range, the denominator represents average value, and the value in bracket represents the number of samples.

Group II inclusion oil and the oil, indicating that Group I inclusion oil corresponds to an apparent higher thermal maturity than Group II inclusion oil and the oil. However, such an interpretation clearly contradicts to the results of inclusion oil maturity calculated by aromatic hydrocarbon compounds aforementioned (Figs. 2 and 6). Indeed, the inclusion oils of YJ-1B, YJ-2B and YJ-3B are composed of both Group I and II inclusion oils, and the corresponding maturity of the inclusion oils calculated by aromatic hydrocarbon compounds should represent an "average" or "mixed" maturity of these inclusion oils. In comparison, the inclusion oil from the YJ-4B sample is composed mainly of Group I inclusion oil, which essentially represents the maturity related to Group I inclusion oil. However, the maturity-related geochemical parameters show an insignificant change trend in the vertical section (Figs. 2 and 6). It can thus be inferred that these
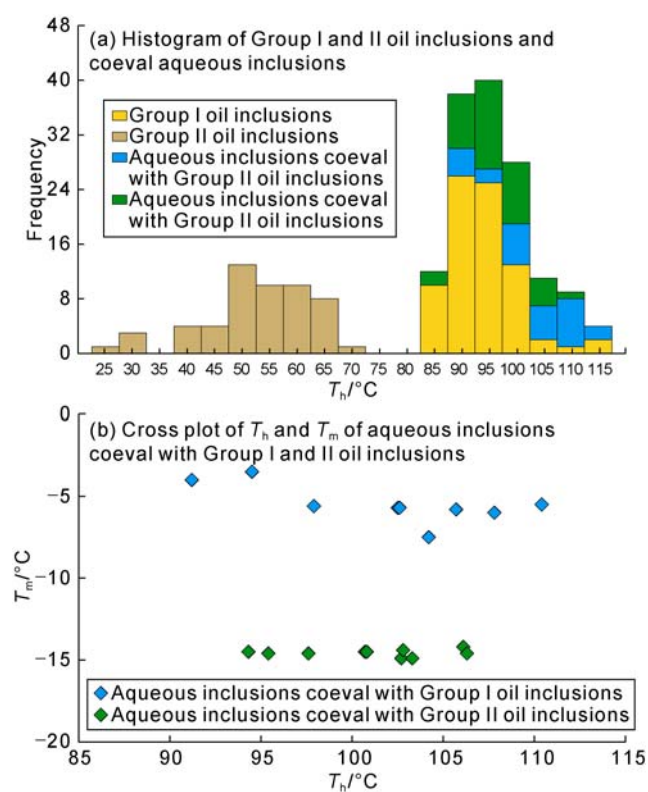

Fig. 11. Microthermometric characteristics of fluid inclusions.

two types of inclusion oils would have similar maturity and represent the same oil charge event.

Cheng et al. [46] and Ma et al. [47] indicated that the reservoir oils in the Shunbei and Yuecan areas have not been affected by biodegradation, water washing, evaporative fractionation or TSR. Therefore, all the above mechanisms cannot be involved in the process of reservoir alteration or destruction. Thermal cracking of oil is another important mechanism for the formation of these two types of oil inclusions. Crustal uplift and denudation and thermal events of magmatism are considered to be the main causes for the abnormal increase in temperature in the Tarim Basin during the Permian [48-49]. One dimensional basin modeling results showed that the current formation temperature represents the maximum value that has ever been experienced by the Ordovician reservoir rocks in the Shunbei area. The formation temperature in the current Ordovician oil reservoir in the Shunbei area is approximately 157.8–162.6 °C [20], close to the threshold temperature for thermal cracking of oil, indicating that the reservoir oils may have undergone slight thermal cracking. Likewise, the current formation temperature in the reservoir of Well YJ1X is 155.27 °C. In this case, severe thermal cracking of the reservoir oil in the oil reservoir in Well YJ1X is unlikely. Ping et al. [50] pointed out that thermal cracking of inclusion oil in the same fluid inclusion assemblage usually causes a "blue shift" in the fluorescence color of oil inclusions and an increase in the relative content of bitumen and vapor filling degrees.

In our current study such features were not observed. Therefore, thermal cracking of reservoir oil/inclusion oil is not the main cause for the formation of Group I and II oil inclusion assemblages.

Fault leakage can cause a sudden and sharp drop in reservoir pressure, resulting in loss of light hydrocarbon components in reservoir oil and precipitation of resin and asphaltene [51–53]. Group I oil inclusion assemblages are composed mainly of diphasic (L_{oil}-V) fluid inclusions at room temperature with vapor filling degrees greater than 10%. During the microthermometric measurements, these oil inclusions homogenize into liquid phase, indicating that these oil inclusions were entrapped as pure liquid phase. The distribution of T_h values of Group I oil inclusions is approximately consistent with that of the coeval aqueous inclusions (Table 1, Fig. 11a), indicating that these oil inclusions were entrapped in a gas-near-saturated state in the oil reservoir [49–50]. Group II oil inclusion assemblages consist mainly of diphasic (S_{bit}-L_{oil}) or triphasic (S_{bit}-L_{oil}-V) fluid inclusions at room temperature with vapor filling degrees of less than 5%. Bitumen in Group II oil inclusions usually occurs along the walls of oil inclusions or is suspended in the oil inclusions, and its relative content gradually increases with depth. Group II oil inclusions commonly change from three phases (S_{bit}-L_{oil}-V) to two phases (S_{bit}-L_{oil}) during microthermometric measurements, suggesting that they may be entrapped by heterogeneous phases. The T_h values of Group II oil inclusions are generally lower than those of the coeval aqueous inclusions (Table 1, Fig. 11a), which may indicate that the entrapped oil is under-saturated with gas [54–55]. The fluorescence characteristics of the oil are similar to that of Group II oil inclusions (Fig. 10). The lower boundary of the present YJ1X oil reservoir is consistent with the occurrence depth range of Group II oil inclusion assemblages (Fig. 2). These evidences would collectively suggest that the oil entrapped by Group II oil inclusions is basically the same as the oil in the present reservoir. Group II oil inclusion assemblages record the occurrence of the last oil charge, adjustment or alteration events inside the reservoir. Compared with Group I oil inclusion assemblage, the occurrence depth range of Group II oil inclusion assemblages is significantly reduced (Fig. 2), which may be caused by light hydrocarbon leakage. The relative contents of resin and asphaltene in the free oils and tricyclic terpenes and pentacyclic triterpenes in the free oils and inclusion oils as a function of depth also indicate that the reservoir oil has undergone gravitational segregation, with heavy resin and asphaltene components gradually accumulating in the lower part of the oil reservoir. Based on the above understandings, it is inferred that some micro-leakage along faults would be the main cause for the formation of the contrasting groups I and II oil inclusion assemblages. Group I oil inclusion assemblages record the charge process of the initial gas-saturated oil, while Group II oil inclusion assemblages reflect the characteristics of the gas-undersaturated oil in the current reservoir after a micro-leakage.

6. Charge history and preservation of the YJ1X oil accumulation

Some Group I oil inclusion assemblages in the C2 calcite cement show typical characteristics of primary fluid inclusions petrographically (Fig. 9c), indicating that the formation time of these oil inclusions may be coeval with the time when C2 cementation occurred. Therefore, the formation time of the C2 calcite cement (425.7±14.0 Ma) can indicate the hydrocarbon charge timing related to Group I oil inclusions. Indeed, hydrocarbon charge timing can be commonly determined by projecting the T_h values of the aqueous inclusions coeval with oil inclusions onto the basin burial history curve [56]. Considering the potential effect of fluid inclusion re-equilibration in calcite [21, 57–59], the minimum value of aqueous inclusions coeval with oil inclusions was chosen to represent its minimum trapping temperature in the present study. The trapping of Group I oil inclusions can thus be interpreted to have occurred in the Early Devonian (T_1, ~415 Ma; Fig. 12), which is quite comparable to the formation age of the C2 calcite cement; while the trapping of Group II oil inclusions occurred in the Middle Devonian (T_2, ~384 Ma), which represents the formation time of the residual/remaining oil reservoir after some gas and light hydrocarbon leakage. Combined with the tectonic evolution history of the study area, the formation and evolution history of the Ordovician ultra-deep reservoir in Well YJ1X can be divided into the following three periods.

6.1. Oil charge period

In the Early Caledonian Orogeny (Cambrian–Early Ordovician), stable platform carbonate strata developed in the Tabei area. Under the influence of unconformity
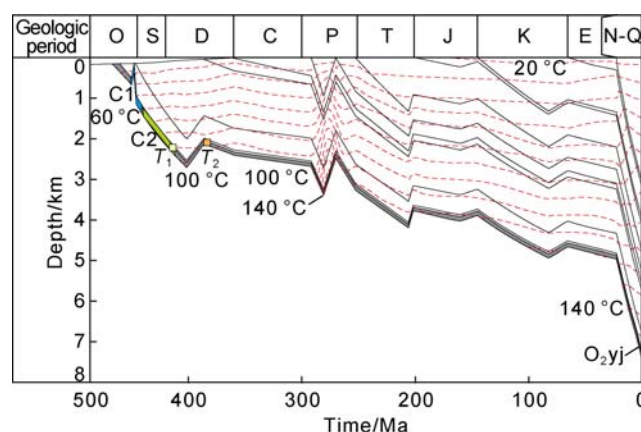

Fig. 12. Burial and thermal history diagram of a typical well in the study area.

related to sedimentary discontinuity and meteoric water karstification, karsting reservoirs were widely developed in the Yuecan area. During the middle Caledonian Orogeny (Ordovician), affected by the overall uplift of the Tazhong and Tabei uplifts, the Yuecan area was characterized by a near north-south trending structural low uplift belt, along with the NE-trending and NW-trending strike-slip faults that cut through the Cambrian strata. In the Late Ordovician, accompanied by the deposition of the Sangtamu Formation (O_3s) mudstone, a complete source-reservoir-cap rock assemblage was in place in the Yuecan area [17, 19, 29]. During the late Caledonian Orogeny (Silurian), a rapid subsidence of the Lower Cambrian Yuertusi Formation ($_1y$) in the Yuecan area promoted the source rock to become mature and generate oils [19-20]. Oils migrated upward along the near vertical strike-slip faults and charged into the Ordovician and Silurian traps to form large-scale oil accumulations. The oil charge event in the reservoir in Well YJ1X occurred approximately 425 Ma, when the equivalent vitrinite reflectance value of the Cambrian source rock reached approximately 0.9%, close to an early oil window. The gas in the oil was close to saturation, and this oil charge event was recorded by Group I oil inclusion assemblages.

6.2. Reservoir leakage period

During the late Caledonian-early Hercynian Orogeny (Silurian-Devonian), the Yuecan area was uplifted as a whole, and a series of large strike-slip faults developed and extended upward to the Middle-Lower Devonian strata [17, 19, 29]. Strong tectonic uplift led to large-scale denudation in this area [60-61]. The overlying Silurian reservoirs experienced severe biodegradation due to their shallowness and lack of high-quality cap rocks, resulting in the widespread occurrence of the Silurian bituminous sandstones [62]. In contrast, the Ordovician oil accumulations underneath in the Yuecan area were not affected by biodegradation, due to their relatively deep burial and excellent preservation conditions. However, tectonic uplift and strike-slip fault activity in this area may have destroyed the integrity of the Ordovician reservoir and caused a sharp drop in formation pressure through the leakage of gas and light hydrocarbons. When the formation pressure dropped to the bubble point pressure of the reservoir oil, the light hydrocarbon components in the reservoir oil would leak upward along the fractures or relatively high-porosity and high-permeability conduits in the cap rocks. The volatilization of the light hydrocarbon components disrupted the equilibrium state of non-polar components in the reservoir oil, causing colloidal molecules to detach from the surface of asphaltene molecules to establish a new thermodynamic equilibrium. At the same time, the asphaltene molecules would flocculate in order to reduce the total surface free energy. When the

degree of flocculation could overcome the Brownian suspension force, they would exsolve and precipitate [51-52]. These exsolved resins and asphaltenes precipitates gradually accumulated to the lower part of the oil reservoir under gravity, resulting in the enrichment of resins and asphaltenes in the lower oil of the reservoir. Therefore, more resins and asphaltenes can be found in the free oils as well as Group II oil inclusions in the lower part of the reservoir in Well YJ1X (Figs. 2 and 9d–9g). In addition, diffusion can also leak gas and light hydrocarbon components during the prolonged geological evolution process, resulting in changes in the composition of the reservoir oil.

6.3. Reservoir preservation period

In the Late Devonian, with an intrusion of seawater into the Yuecan area and the deposition of the Upper Devonian Donghetang Formation, the early Hercynian Orogeny ended [60]. Continued subsidence allowed the preservation of the residual/remaining oil reservoirs, but the oil column height was significantly reduced compared to that at the initial oil charge (Fig. 2). During the middle–late Hercynian Orogeny (Carboniferous–Permian), the Yuecan area changed from a tensional stress setting to a compressional stress setting, along with the development of compressional or compressive strike-slip faults, developing a tectonic pattern similar to that during the early Hercynian Orogeny. The mid-late Hercynian Orogeny is considered to be an important stage of oil charge in the Tabei area. Evidence of large-scale oil charge during this period has been found in the Yingmaili, Halahatang, Tahe and Shunbei oilfields [7, 20, 63–64]. However, the contribution of oil charge during this period to the reservoir in Well YJ1X of the Yuecan area was little or absent with no obvious evidence being found in terms of reservoir geochemistry or oil inclusions. This may be attributed to the following two reasons [61, 65]: Firstly, multiple sets of X-shape conjugate strike-slip faults were developed in the Yuecan area, but their main activation period was in the middle Caledonian to the early Hercynian Orogeny. During the middle-late Hercynian Orogeny, the fault activation was relatively weak, thus the oil charge intensity at this time was correspondingly low; Secondly, Well YJ1X is located on a secondary strike-slip fault, and the reservoir has poor connectivity with the underlying $_1y$ source rock. During the Indosinian-Yanshan Orogeny (Triassic–Cretaceous), the Yuecan area continued to subside as a whole, and multiple episodes of tectonic movements did not exert any significant impact on the area. The present tectonic configuration of the Yuecan area was not developed until the late Himalayan Orogeny (Neogene–Quaternary) [17, 29]. Because of the constantly decreasing heat flow in the Yuecan area [66-67], even though the depth of the Well YJ1X reservoir is more than 7000 m, the present formation temperature of the

oil-producing reservoir interval is only around 155 °C. Under these conditions, the oil remains unaltered, devoid of significant thermal cracking. The formation water in the current reservoir is of $CaCl_2$ type and has a relatively high salinity of 152 358–173 493 mg/L, indicative of a well-preserved, closed hydraulic system. The formation water salinity is similar to that of the aqueous inclusions coeval to Group II oil inclusions (18.0%–18.6%), suggesting that the reservoir in Well YJ1X may have remained as a closed system since the trapping of Group II oil inclusions.

In summary, the reservoir in Well YJ1X only received one oil charge during the Early Devonian (~425 Ma) and has been basically well preserved except for some minor leakage of gas and light hydrocarbons in the Middle Devonian (~384 Ma). The reservoir is characterized by "early and shallow accumulation and late and deep preservation". The preservation of the oil accumulation has been attributed to the stable tectonic environments, low geothermal conditions, and good sealing integrity and capability.

7. Conclusions

The reservoir oil, free (extractable adsorbed) oils and inclusion oils in the Ordovician ultra-deep oil reservoir in Well YJ1X can be classified as one oil family, derived from marine source rocks deposited under similar depositional environments. The reservoir oil, free oils and inclusion oils share similar maturities, with calculated equivalent vitrinite reflectance values in the range of 0.80%–0.96%.

Two types (groups I and II) of oil inclusion assemblages (OIAs) have been identified in the reservoir, of which Group I represents the original gas-saturated oil entering the reservoir during the initial oil charge, whereas Group II represents the undersaturated remaining/residual oil retained in the reservoir after a minor leakage of gas and light hydrocarbons. The Ordovician ultra-deep oil accumulation in Well YJ1X received only one oil charge during the Early Devonian around 425 Ma and has been well preserved after a minor leakage of gas and light hydrocarbons in the Middle Devonian (~384 Ma).

This study demonstrates that primary oil reservoirs can be preserved for over 400 Ma in some ancient craton basins with stable tectonic setting, low geothermal gradients and good sealing of cap rocks. The Ordovician ultra-deep oil accumulation in Well YJ1X is characterized by "early and shallow accumulation and later and deep preservation". The evolution history of the oil accumulation provides some new insights into the charge, emplacement and preservation processes of ultra-deep oil accumulations in the Tarim Basin and elsewhere.

Nomenclature

F_1—methylphenanthrene ratio;

FOI—frequency of oil inclusion, %;

MDR—methyldibenzothiophene ratio;

MPI_1—methylphenanthrene index;

QF_{535}—ratio of the integral area defined by 750 nm and 535 nm to that defined by 535 nm and 430 nm;

T_1—oil charge timing, Ma;

T_2—formation timing of residual reservoir, Ma;

T_h—homogenization temperature, °C;

T_m—final ice melting temperature, °C;

λ_{max}—wavelength at maximum fluorescence intensity, nm.

References

[1] PETERS K E, WALTERS C C, MOLDOWAN J M. The Biomarker Guide: Biomarkers and isotopes in petroleum exploration and earth history. Cambridge: Cambridge University Press, 2005.

[2] DUTKIEWICZ A, RASMUSSEN B, BUICK R. Oil preserved in fluid inclusions in Archaean sandstones. Nature, 1998, 395(6705): 885–888.

[3] JACKSON M J, POWELL T G, SUMMONS R E, et al. Hydrocarbon shows and petroleum source rocks in sediments as old as 1.7×10^9 years. Nature, 1986, 322(6081): 727–729.

[4] BOIS C, BOUCHE P, PELET R. Global geologic history and distribution of hydrocarbon reserves. AAPG Bulletin, 1982, 66(9): 1248–1270.

[5] MILLER R G. The global oil system: The relationship between oil generation, loss, half-life, and the world crude oil resource. AAPG Bulletin, 1992, 76(4): 489–500.

[6] KLEMME H D, ULMISHEK G F. Effective petroleum source rocks of the world: Stratigraphic distribution and controlling depositional factors. AAPG Bulletin, 1991, 75(12): 1809–1851.

[7] NALIVKIN V D, GOL'DBERG I S, KRUGLIKOV N M, et al. Destructive processes affecting oil and gas pools and estimation of the hydrocarbon loss. International Geology Review, 1984, 26(10): 1185–1198.

[8] MACGREGOR D S. Factors controlling the destruction or preservation of giant light oilfields. Petroleum Geoscience, 1996, 2(3): 197–217.

[9] ZHU G Y, ZHANG S C, LIU K Y, et al. A well-preserved 250 million-year-old oil accumulation in the Tarim Basin, western China: Implications for hydrocarbon exploration in old and deep basins. Marine and Petroleum Geology, 2013, 43: 478–488.

[10] BEHAR F, KRESSMANN S, RUDKIEWICZ J L, et al. Experimental simulation in a confined system and kinetic modelling of kerogen and oil cracking. Organic Geochemistry, 1992, 19(1/3): 173–189.

[11] PEPPER A S, DODD T A. Simple kinetic models of petroleum formation. Part II: Oil-gas cracking. Marine and Petroleum Geology, 1995, 12(3): 321–340.

[12] ZHU G Y, ZHANG S C, SU J, et al. The occurrence of ul-

tra-deep heavy oils in the Tabei Uplift of the Tarim Basin, NW China. Organic Geochemistry, 2012, 52: 88–102.

[13] LI Jianzhong, TAO Xiaowan, BAI Bin, et al. Geological conditions, reservoir evolution and favorable exploration directions of marine ultra-deep oil and gas in China. Petroleum Exploration and Development, 2021, 48(1): 52–67.

[14] WEI Guoqi, ZHU Yongjin, ZHENG Jianfeng, et al. Tectonic-lithofacies paleogeography, large-scale source-reservoir distribution and exploration zones of Cambrian subsalt formation, Tarim Basin, NW China. Petroleum Exploration and Development, 2021, 48(6): 1114–1126.

[15] DING Zhiwen, WANG Rujun, CHEN Fangfang, et al. Origin, hydrocarbon accumulation and oil-gas enrichment of fault-karst carbonate reservoirs: A case study of Ordovician carbonate reservoirs in in South Tahe area of Halahatang oilfield, Tarim Basin. Petroleum Exploration and Development, 2020, 47(2): 286–296.

[16] JIA Chengzao, PANG Xiongqi. Research processes and main development directions of deep hydrocarbon geological theories. Acta Petrolei Sinica, 2015, 36(12): 1457–1469.

[17] JIAO Fangzheng. Significance and prospect of ultra-deep carbonate fault-karst reservoirs in Shunbei area, Tarim Basin. Oil & Gas Geology, 2018, 39(2): 207–216.

[18] GU Yi, WAN Yanglu, HUANG Jiwen, et al. Prospects for ultra-deep oil and gas in the "deep burial and high pressure" Tarim Basin. Petroleum Geology and Experiment, 2019, 41(2): 157–164.

[19] QI Lixin. Characteristics and inspiration of ultra-deep fault-karst reservoir in the Shunbei area of the Tarim Basin. China Petroleum Exploration, 2020, 25(1): 102–111.

[20] YANG P, LIU K Y, LIU J L, et al. Petroleum charge history of deeply buried carbonate reservoirs in the Shuntuoguole Low Uplift, Tarim Basin, West China. Marine and Petroleum Geology, 2021, 128: 105063.

[21] GOLDSTEIN R H, REYNOLDS T J. Systematics of fluid inclusions in diagenetic minerals. Broken Arrow: SEPM Society for Sedimentary Geology, 1994.

[22] THIÉRY R, PIRONON J, WALGENWITZ F, et al. Individual characterization of petroleum fluid inclusions (composition and P-T trapping conditions) by microthermometry and confocal laser scanning microscopy: Inferences from applied thermodynamics of oils. Marine and Petroleum Geology, 2002, 19(7): 847–859.

[23] LI K K, GEORGE S C, CAI C F, et al. Fluid inclusion and stable isotopic studies of thermochemical sulfate reduction: Upper Permian and Lower Triassic gasfields, northeast Sichuan Basin, China. Geochimica et Cosmochimica Acta, 2019, 246: 86–108.

[24] LI Q, PARRISH R R, HORSTWOOD M S A, et al. U-Pb dating of cements in Mesozoic ammonites. Chemical Geology, 2014, 376(6): 76–83.

[25] ROBERTS N M W, WALKER R J. U-Pb geochronology of calcite-mineralized faults: absolute timing of rift-related fault events on the northeast Atlantic margin. Geology, 2016, 44(7): 531–534.

[26] NURIEL P, WEINBERGER R, KYLANDER-CLARK A R C, et al. The onset of the Dead Sea transform based on calcite age-strain analyses. Geology, 2017, 45(7): 587–590.

[27] GODEAU N, DESCHAMPS P, GUIHOU A, et al. U-Pb dating of calcite cement and diagenetic history in microporous carbonate reservoirs: Case of the Urgonian Limestone, France. Geology, 2018, 46(3): 247–250.

[28] YANG P, LIU K Y, LI Z, et al. Direct dating Paleo-fluid flow events in sedimentary basins. Chemical Geology, 2022, 588: 120642.

[29] QI Lixin. Oil and gas breakthrough in ultra-deep Ordovician carbonate formations in Shuntuoguole uplift, Tarim Basin. China Petroleum Exploration, 2016, 21(3): 38–51.

[30] HUANG H P, ZHANG S C, SU J. Geochemistry of tri- and tetracyclic terpanes in the Palaeozoic oils from the Tarim Basin, northwest China. Energy & Fuels, 2015, 29(11): 7014–7025.

[31] ZHU G Y, CHEN F R, WANG M, et al. Discovery of the lower Cambrian high-quality source rocks and deep oil and gas exploration potential in the Tarim Basin, China. AAPG Bulletin, 2018, 102(10): 2123–2151.

[32] YU S, PAN C C, WANG J J, et al. Molecular correlation of crude oils and oil components from reservoir rocks in the Tazhong and Tabei uplifts of the Tarim Basin, China. Organic Geochemistry, 2011, 42(10): 1241–1262.

[33] ROBERTS N M W, RASBURY E T, PARRISH R R, et al. A calcite reference material for LA-ICP-MS U-Pb geochronology. Geochemistry, Geophysics, Geosystems, 2017, 18(7): 2807–2814.

[34] VERMEESCH P. Isoplot R: A free and open toolbox for geochronology. Geoscience Frontiers, 2018, 9(5): 1479–1493.

[35] EADINGTON P J, LISK M, KRIEGER F W. Identifying oil well sites: United States patent 5543616. 1996-08-06.

[36] BODNAR R J. Revised equation and table for determining the freezing point depression of H_2O-NaCl solutions. Geochimica et Cosmochimica Acta, 1993, 57(3): 683–684.

[37] DIDYK B M, SIMONEIT B R T, BRASSELL S C, et al. Organic geochemical indicators of palaeoenvironmental conditions of sedimentation. Nature, 1978, 272(5650): 216–222.

[38] CONNAN J, CASSOU A M. Properties of gases and petroleum liquids derived from terrestrial kerogen at various maturation levels. Geochimica et Cosmochimica Acta, 1980, 44(1): 1–23.

[39] HUANG W Y, MEINSCHEIN W G. Sterols as ecological indicators. Geochimica et Cosmochimica Acta, 1979, 43(5): 739–745.

[40] HUGHES W B, HOLBA A G, DZOU L I P. The ratios of dibenzothiophene to phenanthrene and pristane to phytane as indicators of depositional environment and lithology of petroleum source rocks. Geochimica et Cosmochimica Acta, 1995, 59(17): 3581–3598.

[41] RADKE M, WELTE D H, WILLSCH H. Geochemical study on a well in the Western Canada Basin: Relation of the aromatic distribution pattern to maturity of organic matter. Geochimica et Cosmochimica Acta, 1982, 46(1): 1–10.

[42] KVALHEIM O M, CHRISTY A A. TELNÆS N, et al. Maturity determination of organic matter in coals using the methylphenanthrene distribution. Geochimica et Cosmochimica Acta, 1987, 51(7): 1883–1888.

[43] RADKE M, WELTE D H. The Methylphenanthrene Index (MPI): A maturity parameter based on aromatic hydrocarbons: BJOROY M. Advances in Organic Geochemistry 1981. Hoboken: John Wiley and Sons Limited, 1983: 504–512.

[44] BOREHAM C J, CRICK I H, POWELL T G. Alternative calibration of the Methylphenanthrene Index against vitrinite reflectance: Application to maturity measurements on oils and sediments. Organic Geochemistry, 1988, 12(3): 289–294.

[45] MCLIMANS R K. The application of fluid inclusions to migration of oil and diagenesis in petroleum reservoirs. Applied Geochemistry, 1987, 2(5/6): 585–603.

[46] CHENG B, LIU H, CAO Z C, et al. Origin of deep oil accumulations in carbonate reservoirs within the north Tarim Basin: Insights from molecular and isotopic compositions. Organic Geochemistry, 2020, 139: 103931.

[47] MA Anlai, JIN Zhijun, LI Huili, et al. Secondary alteration and preservation of ultra-deep Ordovician oil reservoirs of North Shuntuoguole area of Tarim Basin, NW China. Earth Science, 2020, 45(5): 1737–1753.

[48] LI D X, YANG S F, CHEN H L, et al. Late Carboniferous crustal uplift of the Tarim plate and its constraints on the evolution of the Early Permian Tarim Large Igneous Province. Lithos, 2014, 204: 36–46.

[49] XU Y G, WEI X, LUO Z Y, et al. The early Permian Tarim large igneous province: Main characteristics and a plume incubation model. Lithos, 2014, 204: 20–35.

[50] PING H W, CHEN H H, THIÉRY R, et al. Effects of oil cracking on fluorescence color, homogenization temperature and trapping pressure reconstruction of oil inclusions from deeply buried reservoirs in the northern Dongying Depression, Bohai Bay Basin, China. Marine and Petroleum Geology, 2017, 80: 538–562.

[51] HIRSCHBERG A, DE JONG L N J, SCHIPPER B A, et al. Influence of temperature and pressure on asphaltene flocculation. Society of Petroleum Engineers Journal, 1984, 24(3): 283–293.

[52] HAMMAMI A, PHELPS C H, MONGER-MCCLURE T, et al. Asphaltene precipitation from live oils: An experimental investigation of onset conditions and reversibility. Energy & Fuels, 2000, 14(1): 14–18.

[53] PING H W, LI C Q, CHEN H H, et al. Overpressure release: Fluid inclusion evidence for a new mechanism for the formation of heavy oil. Geology, 2020, 48(8): 803–807.

[54] PIRONON J. Fluid inclusions in petroleum environments: Analytical procedure for PTX Reconstruction. Acta Petrologica Sinica, 2004, 20(6): 1333–1342.

[55] NEDKVITNE T, KARLSEN D A, BJØRLYKKE K, et al. Relationship between reservoir diagenetic evolution and petroleum emplacement in the Ula Field, North Sea. Marine and Petroleum Geology, 1993, 10(3): 255–270.

[56] KARLSEN D A, NEDKVITNE T, LARTER S R, et al. Hydrocarbon composition of authigenic inclusions: Application to elucidation of petroleum reservoir filling history. Geochimica et Cosmochimica Acta, 1993, 57(15): 3641–3659.

[57] LARSON L T, MILLER J D, NADEAU J E, et al. Two sources of error in low temperature inclusion homogenization determination, and corrections on published temperatures for the East Tennessee and Laisvall deposits. Economic Geology, 1973, 68(1): 113–116.

[58] PREZBINDOWSKI D R, TAPP J B. Dynamics of fluid inclusion alteration in sedimentary rocks: A review and discussion. Organic Geochemistry, 1991, 17(2): 131–142.

[59] BOURDET J, PIRONON J, LEVRESSE G, et al. Petroleum type determination through homogenization temperature and vapour volume fraction measurements in fluid inclusions. Geofluids, 2008, 8(1): 46–59.

[60] LIN C S, YANG H J, LIU J Y, et al. Distribution and erosion of the Paleozoic tectonic unconformities in the Tarim Basin, Northwest China: Significance for the evolution of paleo-uplifts and tectonic geography during deformation. Journal of Asian Earth Sciences, 2012, 46: 1–19.

[61] JIAO Fangzheng. Significance of oil and gas exploration in NE strike-slip fault belts in Shuntuoguole area of Tarim Basin. Oil & Gas Geology, 2017, 38(5): 831–839.

[62] ZHANG Jun, PANG Xiongqi, LIU Luofu, et al. Distribution characteristics and petroleum geological significance of the Silurian asphaltic sandstones in Tarim Basin. SCIENCE CHINA Earth Sciences, 2004, 47(S2): 199–208.

[63] CHEN Honghan, WU You, FENG Yong, et al. Timing and chronology of hydrocarbon charging in the Ordovician of Tahe oilfield, Tarim Basin, NW China. Oil & Gas Geology, 2014, 35(6): 806–819.

[64] GU Yi, HUANG Jiwen, JIA Cunshan, et al. Research progress on marine oil and gas accumulation in Tarim Basin. Petroleum Geology and Experiment, 2020, 42(1): 1–12.

[65] TIAN Peng, MA Qingyou, LYU Haitao. Strike-slip faults and their controls on hydrocarbon reservoirs in the Yuecan block of the Northern Tarim Uplift, Tarim Basin. Petroleum Geology and Experiment, 2016, 38(2): 156–161.

[66] LI Huili, QIU Nansheng, JIN Zhijun, et al. Geothermal history of Tarim Basin. Oil & Gas Geology, 2005, 26(5): 613–617.

[67] LIU Yuchen, QIU Nansheng, CHANG Jian, et al. Application of clumped isotope thermometry to thermal evolution of sedimentary basins: A case study of Shuntuoguole area in the Tarim Basin. Chinese Journal of Geophysics, 2020, 63(2): 597–611.